JCTC Journal of Chemical Theory and Computation

Effects of Zero-Point and Thermal Vibrational Averaging on Computed NMR Properties of a Model Compound for Purine Nucleosides

Jeffrey N. Woodford

Department of Chemistry and Biochemistry, Eastern Oregon University, One University Boulevard, La Grande, Oregon 97850-2899

Gerard S. Harbison*

Department of Chemistry, University of Nebraska−Lincoln, Lincoln, Nebraska 68588-0304

Received February 21, 2006

Abstract: A method for the incorporation of thermal averaging into the calculation of nuclear magnetic resonance properties is given. These properties are computed using density functional theory, anharmonic first-order perturbation corrections to a normal-mode analysis, and standard statistical mechanical averaging. The method is applied to the calculation of chemical shieldings and spin−spin coupling constants (*J* couplings) of 1′-imidazolyl-2′-deoxy-β-ribofuranose (IDR), a model compound for purine nucleosides, at the B3LYP/6-311++G(2d,p) level of theory. Thermal averaging causes substantial changes in the values of computed parameters. The calculated harmonic normal modes of IDR are also investigated; we find reasonable agreement with published results from vibrational spectroscopy on DNA fragments. Finally, the calculated magnetic and structural data regarding the reported hydrogen bond between H8 on the imidazole ring and O5′ on the sugar ring are investigated; we find that such data do not strongly support the formation of a hydrogen bond between these two atoms.

Introduction

Nuclear magnetic resonance (NMR) spectroscopy is a primary tool for investigating the structure and dynamics of important biochemical systems.[1] One instance is the study of deoxyribonucleosides with NMR, to obtain data about the conformation and dynamics of the sugar moiety. Many methods have been employed to correlate NMR data with conformations of the deoxyribofuranose ring, including methods based on the Karplus equation,[2,3] the CUPID method,[4,5] and the more recent DORCO method.[6] In all of the above methods, to extract the desired conformational data, it is necessary to have knowledge of the molecule's potential energy surface (PES). With the advent of modern computer equipment and software, it is now common practice to rely on high-quality ab initio or density functional (DFT) calculations to obtain such data. This procedure generally consists of generating a molecular structure of the system of interest, optimizing its structure using a high level of theory and a large basis set, and then adjusting the desired torsion angles to obtain a high-quality PES.

However, the molecular geometry obtained in this way is that of the isolated, vibration-free molecule at 0 K in the gas phase. For typical solid- or liquid-phase samples at room temperature, many vibrational levels are populated, especially low-frequency vibrations, and the measured NMR quantities are actually thermal averages over the zero-point motion and over a Boltzmann distribution of thermally accessible vibrational states. Thus, for a proper comparison between theory and the experiment, a correction accounting for this vibrational averaging must be applied to the theoretical results. This phenomenon is of course intimately related to

* Corresponding author phone: (402) 472-9346; fax: (402) 472-9402; e-mail: gerry@setanta.unl.edu.

10.1021/ct6000736 CCC: $33.50
Published on Web 08/22/2006

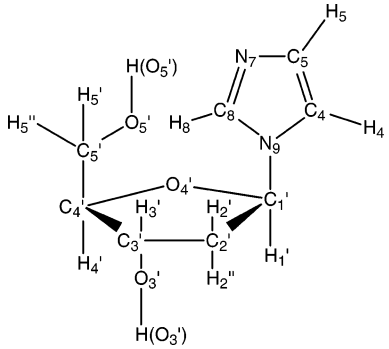

Figure 1. Molecular structure of 1′-imidazolyl-2′-deoxyribofuranose (IDR) and numbering system used.

the well-known primary isotope effect on NMR chemical shifts and *J* couplings, which arises from differences in quantum mechanical vibrational amplitudes and thermal populations resulting from changes in the mass of the nucleus, for which there is vast experimental (for a recent review, see ref 7) and computational[8−11] literature.

It has been known for some time that ensemble averaging over a distribution of microstates should be properly employed in order to achieve suitable agreement with the experiment.[12−14] Most of the previous methods used for averaging have relied upon a combination of molecular dynamics simulations and ab initio or semiempirical calculations. In this work, we present an alternative method for accomplishing the thermal averaging process. In this method, the equilibrium geometry of the molecule of interest, calculated by ab initio means, is displaced along each vibrational coordinate, and the relevant NMR properties are calculated at each displaced geometry. Then, a combination of time-independent perturbation theory and statistical mechanical averaging is applied to the equilibrium and displaced computational results. We present a detailed theoretical treatment of this method as it is applied to the calculation of thermally averaged chemical shieldings and spin−spin coupling constant (SSCC) values, along with the results of this method as they are applied to 1′-imidazolyl-2′-deoxy-β-ribofuranose (IDR; Figure 1), an analogue of purine DNA bases. It has been shown that IDR is the minimum structural unit required to correctly model the furanose moiety of purine nucleosides, because of extensive coupling between the base and the sugar ring.[15] Furthermore, IDR does not have charged atoms, such as those in a phosphate group, to avoid complications arising from the selection and proper placement of the counterion(s).[16]

Many previous authors have conducted theoretical investigations on DNA base model systems. Typically, however, only a small part of a nucleoside is modeled, appropriate for the particular study. For instance, Lluch et al.[17−19] have theoretically examined dimers of the model compound 7-azaindole as a model system for excited-state proton transfer between DNA base pairs. The formamidine−formamide complex has been used to mimic the A−T hydrogen-bonding interaction.[20] Dimethyl phosphate is often used as a model compound to represent the DNA/RNA backbone.[21,22] To model entire nucleosides, either a fragmentation scheme is employed[23] or a relatively low level of theory, either HF or semiempirical methods, must be used.[24] Similarly, many previous workers have employed vibrational averaging techniques on ab initio derived magnetic properties. For instance, Del Bene et al.[25,26] have theoretically examined SSCCs for hydrogen-bonded complexes, with the inclusion of full vibrational averaging; Bühl and Grigoleit[27] have examined vibrational corrections to chemical shifts of transition metal complexes; and Barone et al.[28] used a hybrid ab initio/semiempirical method to incorporate vibrational averaging into two different conformers of β-alanine. These studies, however, have typically involved either a small number of atoms or selectively including only certain vibrations in the averaging process. (A notable exception is the work by Case.[29]) The present work, on the other hand, represents the result of advanced ab initio computations on a model compound representing an entire nucleoside unit, including full vibrational averaging.

Theory

To obtain the thermally averaged chemical shielding $\bar{\sigma}(T)$, we proceed according to the following strategy. First, the molecule of interest is fully optimized with a large basis set, and a harmonic frequency analysis is performed at the equilibrium geometry. Then, the molecule is displaced along each normal mode between $-\alpha$ and $+\alpha$, where α is the characteristic length of the vibration ($\alpha = \sqrt{\hbar/\mu\omega_0}$ with μ being the reduced mass and ω_0 the harmonic frequency of the vibration), and the potential energy is fitted to a fourth-order polynomial.

$$E_j(y) = \beta_j y^2 + \gamma_j y^3 + \delta_j y^4 \tag{1}$$

Here $y = x/\alpha$ and the index j runs from 1 to $M = 3N - 6$, the number of normal modes. The harmonic portion of the vibration is contained in the β_j term, while the anharmonicity is contained in the γ_j and δ_j terms.

Next, for each mode, the chemical shielding for each atom is calculated at each displaced geometry and fitted to a second-order polynomial. For the *A*th atom displaced along the *j*th vibrational mode, the chemical shielding is given by the following expression.

$$\sigma_j^{(A)}(y) = \sigma_0^{(A)} + \sigma_{1j}^{(A)} y + \sigma_{2j}^{(A)} y^2 \tag{2}$$

The quantity $\sigma_0^{(A)}$ represents the electronic contribution to the chemical shielding and is independent of molecular vibration; $\sigma_1^{(A)}$ and $\sigma_2^{(A)}$ represent the linear and quadratic corrections to the chemical shielding, respectively, due to vibration. In principle, additional correction terms (e.g., cubic) may be required in order to correctly model the data; however, in the present study, we found that truncation at the quadratic term yielded excellent results. Of course, in higher-symmetry molecules, only the fully symmetric modes would possess linear coefficients; the present molecule is unfortunately C_1.

Following the determination of these coefficients, first-order perturbation theory is applied to determine the expectation values of E_j, $\sigma_1^{(A)}y$, and $\sigma_2^{(A)}y^2$ in the *n*th vibrational state. When $\hat{H}_j' = \gamma_j\hat{y}^3 + \delta_j\hat{y}^4$ is used as the perturbation

Hamiltonian and the harmonic oscillator wave functions are used as a basis, the following results are obtained.

$$E_{jn} = E_{jn}^{(0)} + E_{jn}^{(1)} = \left(n + \frac{1}{2}\right)\hbar\omega_{0j} + \left(n^2 + n + \frac{1}{2}\right)\delta_j \quad (3)$$

$$\langle\sigma_{1j}^{(A)}\rangle_n = \frac{\langle\psi_n^{(0)} + \psi_n^{(1)}|\sigma_{1j}^{(A)}\hat{y}|\psi_n^{(0)} + \psi_n^{(1)}\rangle}{\langle\psi_n^{(0)} + \psi_n^{(1)}|\psi_n^{(0)} + \psi_n^{(1)}\rangle}$$

$$= \frac{\sigma_{1j}^{(A)}\left(\sum_{m\neq n} c_{j,nm}^{(1)}\langle\psi_n^{(0)}|\hat{y}|\psi_m^{(0)}\rangle + \sum_{m\neq n} c_{j,nm}^{(1)}\langle\psi_m^{(0)}|\hat{y}|\psi_n^{(0)}\rangle + \sum_{m\neq n}\sum_{b\neq n} c_{j,nm}^{(1)}c_{j,nb}^{(1)}\langle\psi_m^{(0)}|\hat{y}|\psi_b^{(0)}\rangle\right)}{1 + \sum_{m\neq n}|c_{j,nm}^{(1)}|^2} \quad (4)$$

$$\langle\sigma_{2j}^{(A)}\rangle_n = \frac{\langle\psi_n^{(0)} + \psi_n^{(1)}|\sigma_{2j}^{(A)}\hat{y}^2|\psi_n^{(0)} + \psi_n^{(1)}\rangle}{\langle\psi_n^{(0)} + \psi_n^{(1)}|\psi_n^{(0)} + \psi_n^{(1)}\rangle}$$

$$= \frac{\sigma_{2j}^{(A)}\left[\left(n + \frac{1}{2}\right) + \sum_{m\neq n} c_{j,nm}^{(1)}\langle\psi_n^{(0)}|\hat{y}^2|\psi_m^{(0)}\rangle + \sum_{m\neq n} c_{j,nm}^{(1)}\langle\psi_m^{(0)}|\hat{y}^2|\psi_n^{(0)}\rangle + \sum_{m\neq n}\sum_{b\neq n} c_{j,nm}^{(1)}c_{j,nb}^{(1)}\langle\psi_m^{(0)}|\hat{y}^2|\psi_b^{(0)}\rangle\right]}{1 + \sum_{m\neq n}|c_{j,nm}^{(1)}|^2} \quad (5)$$

In the above equations, $c_{j,nm}^{(1)}$ is the usual set of expansion coefficients of the first-order wave function in terms of the basis functions for the jth mode.

$$c_{j,nm}^{(1)} = \frac{\langle\psi_m^{(0)}|\hat{H}_j'|\psi_n^{(0)}\rangle}{E_{jn}^{(0)} - E_{jm}^{(0)}} = \frac{\gamma_j\langle\psi_m^{(0)}|\hat{y}^3|\psi_n^{(0)}\rangle}{\hbar\omega_{0j}(n-m)} + \frac{\delta_j\langle\psi_m^{(0)}|\hat{y}^4|\psi_n^{(0)}\rangle}{\hbar\omega_{0j}(n-m)} \quad (m\neq n) \quad (6)$$

While the sums in eqs 4 and 5 are infinite, they can be solved in closed form; expressions for these sums are given in the Appendix.

The correction to the chemical shielding due to zero-point vibration (ZPV) is then calculated by summing the contributions of the ground vibrational state for each mode.

$$\bar{\sigma}_{\mathrm{ZPV}}^{(A)} = \sum_{j=1}^{M}(\langle\sigma_{1j}^{(A)}\rangle_0 + \langle\sigma_{2j}^{(A)}\rangle_0) \quad (7)$$

The correction to the chemical shielding due to the thermal population of excited vibrational states is then calculated by taking the statistical mechanical average over the thermally accessible vibrational levels. Assuming no coupling between modes, this correction is given by

$$\bar{\sigma}_{\mathrm{thermal}}^{(A)}(T) = \sum_{j=1}^{M}\frac{1}{q_j}\sum_{n=0}^{\infty}[(\langle\sigma_{1j}^{(A)}\rangle_n - \langle\sigma_{1j}^{(A)}\rangle_0) + (\langle\sigma_{2j}^{(A)}\rangle - \langle\sigma_{2j}^{(A)}\rangle_0)]\exp(-\Delta E_{jn}/kT) \quad (8)$$

where k is Boltzmann's constant, T is the absolute temperature, ΔE_{jn} is the difference in energy for the jth mode from the ground vibrational state to the nth state, and q_j is the thermal part of the vibrational partition function for the jth mode.

$$q_j = \sum_{n=0}^{\infty}\exp(-\Delta E_{jn}/kT) \quad (9)$$

Finally, the overall thermal average of the chemical shielding for the Ath atom is taken by summing the electronic contribution, the zero-point vibrational contribution, and the thermal excitation contribution.

$$\bar{\sigma}^{(A)}(T) = \sigma_0^{(A)} + \bar{\sigma}_{\mathrm{ZPV}}^{(A)} + \bar{\sigma}_{\mathrm{thermal}}^{(A)}(T) \quad (10)$$

For purposes of comparison, these values were also calculated using the unperturbed, purely harmonic Hamiltonian. These expressions are

$$\bar{\sigma}_{\mathrm{ZPV,harmonic}}^{(A)} = \frac{1}{2}\sum_{j=1}^{M}\sigma_{2j}^{(A)} \quad (11)$$

$$\bar{\sigma}_{\mathrm{thermal,harmonic}}^{(A)} = \sum_{j=1}^{M}\left[\sigma_{2j}^{(A)}\frac{\exp(-\hbar\omega_{0j}/kT)}{1 - \exp(-\hbar\omega_{0j}/kT)}\right] \quad (12)$$

It is $\bar{\sigma}^{(A)}(T)$ which is then compared to the experiment. To compute a thermally averaged scalar coupling value $\bar{J}^{(a)}(T)$ for the ath coupling constant, the same procedure was followed. The corresponding equations are given as eqs 13−15.

$$\bar{J}_{\mathrm{ZPV}}^{(a)} = \sum_{j=1}^{M}(\langle J_{1j}^{(a)}\rangle_0 + \langle J_{2j}^{(a)}\rangle_0] \quad (13)$$

$$\bar{J}_{\mathrm{thermal}}^{(a)}(T) = \sum_{j=1}^{M}\frac{1}{q_j}\sum_{n=0}^{\infty}[(\langle J_{1j}^{(a)}\rangle_n - \langle J_{1j}^{(a)}\rangle_0) + (\langle J_{2j}^{(a)}\rangle - \langle J_{2j}^{(a)}\rangle_0)]\exp(-\Delta E_{jn}/kT) \quad (14)$$

$$\bar{J}^{(a)}(T) = J_0^{(a)} + \bar{J}_{\mathrm{ZPV}}^{(a)} + \bar{J}_{\mathrm{thermal}}^{(a)}(T) \quad (15)$$

Computational Details

All calculations were performed on a 16-node Beowulf cluster running Linux. Geometry optimizations and vibrational frequency calculations were performed with GAMESS.[30] The structure of IDR was optimized using delocalized internal coordinates[31] and DFT with the B3LYP functional[32] and the 6-311++G(2d,p) basis set. Optimization was continued until each member of the Cartesian gradient vector was less than or equal to 1.0×10^{-6} Hartree/bohr. Chemical shift and scalar coupling values were calculated using Gaussian 03[33] also at the B3LYP/6-311++G(2d,p) level of theory and the "tight" criterion for the self-consistent field density.

The chemical shielding values calculated at the equilibrium geometry were used to obtain σ_0 of eq 1. To obtain γ_j, δ_j, $\sigma_1^{(A)}$, $\sigma_2^{(A)}$, $J_1^{(a)}$, and $J_2^{(a)}$, first, four displacements between $-\alpha$ and $+\alpha$ were calculated along each normal coordinate and the energy, chemical shielding, and SSCC values were

Table 1. Selected Calculated Bond Lengths and Valence Angles for IDR[a]

property	value	property	value
C1′−O4′	1.428	C5′−C4′−C3′	115.1
C4′−O4′	1.432	O4′−C1′−N9	109.7
C1′−N9	1.447	C2′−C1′−N9	114.9
C1′−C2′	1.533	O5′−C5′−C4′	109.9
C2′−C3′	1.520	C1′−N9−C4	125.9
C3′−C4′	1.544	τ_0 (C4′−O4′−C1′−C2′)	−15.4
C3′−O3′	1.431	τ_1 (O4′−C1′−C2′−C3′)	29.8
C4′−C5′	1.520	τ_2 (C1′−C2′−C3′−C4′)	−31.9
C5′−O5′	1.427	τ_3 (C2′−C3′−C4′−O4′)	23.7
C1′−C2′−C3′	103.1	τ_4 (C3′−C4′−O1′−C2′)	−5.3
C2′−C3′−C4′	102.8	β	162.5
C3′−C4′−O4′	106.5	γ	51.5
C4′−O4′−C1′	111.1	δ	146.0
O4′−C1′−C2′	105.8	ϵ	−66.1
C2′−C3′−O3′	107.6	χ	243.9
C4′−C3′−O3′	111.8		

[a] Bond lengths in angstroms; valence angles and torsion angles in degrees.

calculated at the displaced coordinates. For the 69 normal modes of IDR, this procedure resulted in 276 separate chemical shielding/SSCC calculations. In addition, for a few modes, more than four displacements were required to obtain reliable fitted values of the energy; these additional displacements were evaluated between -0.5α and $+0.5\alpha$. Then, the calculated energy values for each mode were fitted to a fourth-order polynomial with the linear term set equal to zero, and the calculated chemical shielding and SSCC values for each mode were fitted to quadratic polynomials. In all cases, the fitting procedures led to correlation coefficients (R^2) greater than or equal to 0.99, thereby justifying the expansion of the chemical shielding/SSCC data only through second order in vibrational displacement. Equations 7−10 were then applied to find the thermally averaged chemical shielding values. An analogous procedure was used for the SSCC data.

In eqs 8 and 9, because the perturbed energy difference ΔE_{jn} contains terms proportional to n^2, the infinite sums over n are only conditionally convergent. Thus, the sum does not have a closed-form solution and must be truncated. We found that truncation at $n \sim 50$ yielded values that were sufficiently converged. In all cases, the calculations were repeated for a maximum value of n of 100; we found the error due to truncation was negligible.

All of the post-electronic structure calculations were performed with an in-house program written in C. Data files and the computer program code may be found in the Supporting Information.

Results and Discussion

Figure 1 shows the B3LYP/6-311++G(2d,p)-optimized geometry of IDR, along with the numbering scheme employed in the current study. The numbering scheme was chosen to be consistent with the numbering for purine DNA bases. In general, several conformers of IDR are possible; we have chosen the lowest-energy conformation found in B-DNA, of C2′-endo/anti.[34] Table 1 shows selected structural data obtained for IDR. One can see that DFT predicts reasonable values for the bond lengths, valence angles, and torsion angles presented. The bond lengths tend to be higher than those predicted at the MP2/6-31G(d) level of theory[10] and also higher compared to crystal structure data on B-DNA; however, the discrepancy is not bad considering the strong crystal packing forces present in DNA crystals which are not accounted for in the theoretical calculations. The agreement in valence angles between the DFT, MP2, and crystal structure results is excellent.

The predicted torsion angles are also in line with those found for B-DNA, with the exception of β and ϵ; these values are outside the ranges traditionally found for B-DNA. This is most likely due to the lack of phosphate groups at the O3′ and O5′ positions in our model compound. In particular, the important glycosidic torsion angle, χ, is well-predicted by the present calculations; B-DNA normally exhibits χ values in the range of 252° ± 23°, and the calculated value of 243.9° is well within these error limits. Furthermore, the pseudorotation amplitude and phase angle, obtained using the method of Altona and Sundaralingam,[35] are 32.3° and 170.6°, respectively; these values are reasonable for a C2′-endo (south) structure and within values normally found for B-DNA.

Previous authors have commented on the C8−H8···O5′ "hydrogen bond" conferring stability on the anti conformer as opposed to the syn conformer for rotation about χ.[36−38] In the present work, we find a H8···O5′ distance of 2.685 Å and a C8···O5′ distance of 3.576 Å. In our estimation, these interatomic distances are too large in order for this interaction to be properly considered a "hydrogen bond". This view is bolstered by the fact that the calculated C8−H8 bond length, 1.078 Å, is virtually identical with the calculated C4−H4 and C5−H5 bond lengths (1.078 and 1.077 Å, respectively), which do not participate in any sort of hydrogen bond. If the H8−O5′ interaction were a true hydrogen bond, one would expect a lengthening of the C8−H8 bond compared to comparable C−H bonds as a result of this interaction. Indeed, it is this structural feature that is a key indicator of a traditional hydrogen bond. One might argue that the C8−H8···O5′ interaction is a recently discovered "blue-shifting hydrogen bond",[39] in which the C−H bond actually shortens and the C−H stretching frequency, ν(C−H), increases upon complexation. We do not find any shortening of the C8−H8 bond either, and ν(C8−H8) lies directly between the C4−H4 and C5−H5 symmetric and asymmetric stretching frequencies, where an "ordinary" C−H bond stretch would be expected to lie. If this is a "blue-shifting" hydrogen bond, the blue shift in stretching frequency in this case is exceedingly small. Finally, our calculated NMR SSCC data do not indicate the presence of any significant through-bond coupling between H8 and C5′. In our opinion, while this interaction may technically satisfy many criteria of a rigorous hydrogen-bonding analysis based on atoms-in-molecules principles,[40] we believe this interaction should more properly be characterized as a weak dipolar interaction between a slightly electropositive hydrogen atom (H8) and an electronegative oxygen atom (O5′), and the stability of the anti conformer over that of the syn conformer in DNA is most likely due to a number of contributions, including

this weak dipolar interaction, steric effects, and numerous other structural modifications associated with binding in DNA. It is worth pointing out that, in the gas phase, it appears that the syn conformer of 2′-deoxyguanosine is energetically more stable,[41] again owing to the weakness of the C8−H8•••O5′ interaction.

Table 2 displays the calculated B3LYP/6-311++G(2d,p) harmonic vibrational frequencies for IDR above 800 cm^{-1}. The lack of an imaginary harmonic frequency illustrates that the optimized structure is at a minimum on the potential energy surface. Also presented in Table 2 are the contributions to each mode from the molecule's natural internal coordinates, as determined by the method of Boatz and Gordon[42] and by visual inspection of each mode. Because the molecule lacks symmetry, there are very few modes consisting of only a small number of internal coordinates; modes below 800 cm^{-1} tend to be highly delocalized, with no individually large contribution from even a small number of internal coordinates. The exceptions are ν_1, calculated at 39 cm^{-1}, which is identified as the glycosidic rotation mode (χ), and ν_3, at 96 cm^{-1}, which is identified as the sugar ring puckering mode. Even these two modes, however, are not "pure" χ-rotation or pseudorotation modes; there is substantial mixing in all of the low-energy modes with many low-energy vibrational features, including C1′−N9 torsion and furanose ring torsions. Surprisingly, there are few published theoretical calculations of purine deoxyribonucleosides at the DFT level with large basis sets. Our results are in reasonable agreement with the ones already published,[43,44] considering the different levels of theory and different basis sets employed in those studies.

However, to truly assess the validity of the calculated numbers, especially with regard to the deoxyribose moiety, a comparison to experimental data is required. The proper comparison should be to deoxyribose vibrations of purine bases in DNA, especially because gas-phase vibrational data on individual purine deoxyribonucleosides are unfortunately scarce.[45−47] (However, our results are in substantial agreement with the existing gas-phase vibrational data that appear in the literature.) There are many well-known DNA vibrations arising from the sugar ring; most of the prominent ones appear in the 800−1500 cm^{-1} frequency range, with vibrations in the higher frequencies of this range corresponding to ones that are coupled between the base and sugar rings. A compendium of solution-phase Fourier transform infrared results on DNA fragments has recently been published.[48] The prominent vibrations arising from the deoxyribose ring occur at 1221, 1135, 1116−1119, 1044−1069, 1010−1020, 950−970, 890−899, and 820−842 cm^{-1}. Of these eight vibrational bands, we are able to successfully reproduce the first seven of them, considering that DFT, and ab initio calculations in general, tend to overestimate vibrational frequencies. For the lowest-energy experimental vibrational band, we are unable to find a corresponding one predicted from the calculations; however, because this vibration involves vibration between the oxygen atoms and the phosphate groups, such disagreement is not surprising.

We calculate a deoxyribose vibration at 1229 cm^{-1}, corresponding to the experimental 1221 cm^{-1} vibration. This

Table 2. Calculated Harmonic Vibrational Frequencies above 800 cm^{-1} and Their Descriptions[a]

mode	harmonic frequency (cm^{-1})	description
ν_{21}	807	δ(C1′−C2′−C3′)
ν_{22}	838	H8, H5 out-of-plane bends (symmetric)
ν_{23}	859	H8, H5 out-of-plane bends (asymmetric)
ν_{24}	880	τ(C2′−C3′) + τ(C3′−C4′) (symmetric)
ν_{25}	888	τ(C2′−C3′) + τ(C3′−C4′) (asymmetric)
ν_{26}	914	imidazole ring breathing mode (asymmetric)
ν_{27}	923	τ(C1′−C2′) + τ(C3′−C4′)
ν_{28}	945	furanose ring breathing mode
ν_{29}	993	furanose ring bending mode (asymmetric)
ν_{30}	1005	furanose ring bending mode (symmetric)
ν_{31}	1050	imidazole ring bending mode
ν_{32}	1057	ν(C1′−C2′) + ν(C2′−C3′) (asymmetric)
ν_{33}	1088	ν(C3′−O3′) + ν(C5′−O5′) (asymmetric)
ν_{34}	1108	ν(C3′−O3′) + ν(C5′−O5′) (symmetric)
ν_{35}	1109	ν(C1′−O4′) + ν(C4′−O4′) (symmetric)
ν_{36}	1116	ν(C1′−O4′) + ν(C4′−O4′) (asymmetric)
ν_{37}	1130	ν(C−O) in furanose ring coupled to ν(C−N) in imidazole ring
ν_{38}	1196	δ(H−O3′−C3′) + δ(H−O5′−C5′) (asymmetric)
ν_{39}	1210	δ(H−O3′−C3′) + δ(H−O5′−C5′) (symmetric)
ν_{40}	1229	C2′−H_2 twist + ν(C3′−O3′)
ν_{41}	1247	ν(C−N) in imidazole ring
ν_{42}	1278	ν(C1′−N9) + ν(C8−N9) + ν(C4−N9) (asymmetric)
ν_{43}	1285	ν(C1′−N9) + ν(C8−N9) + ν(C4−N9) (asymmetric)
ν_{44}	1312	coupled furanose + imidazole stretch mode
ν_{45}	1332	H3′ rock
ν_{46}	1337	coupled furanose + imidazole stretch mode
ν_{47}	1354	furanose CH rocking + asymmetric ν(C3′−C4′) + ν(C4′−O4′)
ν_{48}	1360	furanose ring deformation
ν_{49}	1386	ν(C1′−N9)+ imidazole ring breathing
ν_{50}	1390	ν(C2′−C3′)+ ν(C3′−C4′) (asymmetric)
ν_{51}	1424	ν(C2′−C3′)+ ν(C3′−C4′) (symmetric)
ν_{52}	1454	ν(C4′−C5′)
ν_{53}	1470	C2′−H_2 scissor mode
ν_{54}	1489	C2′−H_2 scissor mode
ν_{55}	1505	C5′−H_2 scissor mode
ν_{56}	1515	ν(N7−C8)+ ν(N7−C6) (asymmetric)
ν_{57}	1541	ν(N7−C8)+ ν(C4−C5)
ν_{58}	2979	ν(C5′−H5′)+ ν(C5′−H5″) (symmetric)
ν_{59}	3010	ν(C4′−H4′)
ν_{60}	3034	ν(C5′−H5′)+ ν(C5′−H5″) (asymmetric)
ν_{61}	3043	ν(C3′−H3′)
ν_{62}	3058	ν(C1′−H1′)
ν_{63}	3086	ν(C2′−H2′)+ ν(C2′−H2″) (symmetric)
ν_{64}	3134	ν(C2′−H2′)+ ν(C2′−H2″) (asymmetric)
ν_{65}	3235	ν(C4−H4)+ ν(C5−H5) (asymmetric)
ν_{66}	3250	ν(C8−H8)
ν_{67}	3264	ν(C4−H4)+ ν(C5−H5) (symmetric)
ν_{68}	3819	ν(O3′−H)
ν_{69}	3842	ν(O5′−H)

[a] δ = valence angle, ν = linear displacement (stretch), τ = torsion.

Table 3. Selected Calculated Carbon and Hydrogen Chemical Shielding (σ) Values for IDR at 298 K

atom	$\sigma_0^{(A)}$	$\bar{\sigma}_{ZPV}^{(A)}$	$\bar{\sigma}_{thermal}^{(A)}$	$\bar{\sigma}^{(A)}$	$\bar{\sigma}_{ZPV,harmonic}^{(A)}$	$\bar{\sigma}_{thermal,harmonic}^{(A)}$	$\bar{\sigma}_{harmonic}^{(A)}$
C1′	88.8259	−1.9918	−0.1608	86.6733	−1.2695	−0.2489	87.3075
C2′	137.4698	−4.4233	−0.1180	132.9285	−2.4228	−0.5198	134.5272
C3′	101.5792	−4.0187	−0.4640	97.0965	−2.0890	−0.7185	98.7718
C4′	87.7574	−6.6294	−0.4139	80.7140	−2.5422	−1.2407	83.9744
C5′	113.4706	−7.9713	−0.7875	104.7118	−2.8484	−1.9584	108.6638
N9	47.2250	−3.1595	−1.2149	42.8506	−2.8739	−1.8335	42.5176
H1′	25.7170	−0.4174	−0.0290	25.2706	−0.1970	−0.0321	25.4879
H2′	29.2808	−0.5247	−0.0789	28.6772	−0.2696	−0.0696	28.9416
H2″	29.6026	−0.4345	−0.0568	29.1113	−0.2570	−0.0632	29.2823
H3′	27.2119	−0.5948	−0.0496	26.5675	−0.2632	−0.0549	26.8938
H(O3′)	31.5791	−4.1908	−0.1429	27.2454	−0.9588	−0.7009	29.9195
H4′	27.9921	−0.3482	−0.0296	27.6143	−0.2188	−0.0117	27.7616
H5′	27.8037	−0.9491	−0.0605	26.7940	−0.3463	−0.1822	27.2753
H5″	27.9183	−0.8501	−0.0825	26.9857	−0.3470	−0.1606	27.4107
H(O5′)	31.5991	−10.2818	−0.2810	21.0363	−1.5921	−2.8101	27.1969

vibration consists mostly of a C3′−O3′ stretch and a twisting motion of the hydrogen atoms on C2′. We calculate three vibrations clustered at 1108, 1109, and 1116 cm^{-1}, having large calculated IR intensities, corresponding to the two experimental IR bands at 1116−1119 and 1135 cm^{-1}. These bands are experimentally observed to be strong, and they consist mainly of C−C and C−O stretches. We calculate two vibrations at 1057 and 1088 cm^{-1}, corresponding to the two experimental IR bands at 1044−1069 and 1010−1020 cm^{-1}. Again, these vibrations consist of C−O vibrations, both symmetric and asymmetric. We find two vibrations at 1005 and 993 cm^{-1} that consist of symmetric and asymmetric furanose ring-bending modes, which we assign to the observed IR bands between 950 and 970 cm^{-1}. Finally, we calculate several lower-energy vibrations involving the ribose ring, mainly involving stretches and torsions involving the C2′−C3′, C3′−C4′, and C4′−C5′ bonds; their energies are at 945, 923, 888, and 880 cm^{-1}. We assign these modes to the ones observed between 890 and 899 cm^{-1}. It is also noteworthy that we are able to predict some vibrational modes in the purine ring, even though IDR is not an actual purine deoxyribonucleoside. These modes are at 1515 cm^{-1}, involving the C5/C8−N7 symmetric stretch (observed: 1476−1495 cm^{-1}), and at 1386 cm^{-1}, involving an imidazole breathing mode coupled to the C1′−N9 stretch (observed: 1369−1381 cm^{-1}).

In Table 3 are presented the calculated chemical shielding values for carbon, hydrogen, and nitrogen atoms at the equilibrium geometry of IDR and the thermally averaged chemical shielding values obtained from eq 10 using both harmonic and anharmonic contributions to the shielding. Also presented are the chemical shielding values assuming each vibration is purely harmonic, calculated using eqs 11 and 12. Considering first the equilibrium geometry values, we see that the chemical shieldings of C1′ and C4′, the carbons bonded to O4′, are large compared to those of C2′, C3′, and C5′, with C1′ being the most deshielded because it is adjacent to two electronegative atoms, O4′ and N9. The trend for the hydrogen chemical shifts also follows the usual pattern, with the hydroxyl protons being the most shielded and H1′, the proton adjacent to the strongly deshielded C1′, itself being the most deshielded.

Table 4 presents selected calculated one-bond, two-bond, and three-bond J coupling data for the equilibrium geometry of IDR, as well as their thermally averaged values using eq 15 employing first-order perturbation theory and using the harmonic oscillator approximation. We focus mainly on the NMR properties of the furanose ring, so J couplings involving just the imidazole ring are excluded. Among one-bond coupling constants, as expected, atom C1′ exhibits both the strongest homonuclear and heteronuclear coupling constants because C1′ is so deshielded compared to other carbons. Consequently, $^1J_{C2'C3'}$ is comparatively small, and the heteronuclear couplings $^1J_{C2'H2''}$ and $^1J_{C3'H3''}$ are large. The hydrogen ^3J values also show evidence of strong coupling between C1′ and C2′, with $^3J_{H1'H2'} = 5.7$ Hz and $^3J_{H1'H2''} = 8.4$ Hz, both values being unusually large compared to the other H−H ^3J values.

As a typical example of the thermal averaging process, the carbon and hydrogen chemical shift data are presented in Table 5 for IDR displaced along ν_{69}, the O5′−H5′ stretch mode. Clearly, the effect of vibrational displacement is greatest on H5′, the atom which is the most substantially displaced, and on C5′, H5′, and H5″, the methylene group adjacent to O5′. Also shown in Table 5 are $\sigma_{1,j=69}^{(A)}$ and $\sigma_{2,j=69}^{(A)}$, the fitting parameters obtained after fitting the chemical shift data to eq 2 for this mode. Shown in Figure 2 is the chemical shift for H5′ as a function of vibrational displacement, along with the quadratic fitting function. The correlation coefficient for this fit is greater than 0.9999. In this particular example, $\sigma_j^{(A)}(y)$ is a decreasing function of α; however, this is not generally the case. An inspection of the data in Table 5 reveals that $\sigma_j^{(A)}(y)$, in general, does not have any preferred dependence on α, other than approximately quadratic.

Once the linear and quadratic fitting coefficients are obtained for each chemical shielding value and each J coupling, eqs 7 and 13 may then be applied to obtain $\bar{\sigma}_{ZPV}^{(A)}$ and $\bar{J}_{ZPV}^{(a)}$, the corrections to the chemical shielding and J coupling, respectively, due to ZPV. These ZPV corrections are presented in column three of Tables 3 and 4, respectively. Turning first to $\bar{\sigma}_{ZPV}^{(A)}$, we see that the effect of ZPV correction is to decrease σ compared to its vibration-free,

Table 4. Selected Calculated *J* Coupling Data for IDR at 298 K[a]

N	bond path	$J_0^{(a)}$	$\bar{J}_{ZPV}^{(a)}$	$\bar{J}_{thermal}^{(a)}$	$\bar{J}^{(a)}$	$\bar{J}_{ZPV,harmonic}^{(a)}$	$\bar{J}_{thermal,harmonic}^{(a)}$	$\bar{J}_{harmonic}^{(a)}$
1	$^1J_{C1'C2'}$	35.773	0.650	0.053	36.477	0.284	0.065	36.122
2	$^1J_{C1'H1'}$	150.667	1.966	0.315	152.948	2.474	0.306	153.447
3	$^1J_{C1'N9}$	8.437	0.082	−0.180	8.338	0.002	−0.236	8.202
4	$^1J_{C2'C3'}$	36.470	0.094	0.011	36.575	0.187	−0.085	36.572
5	$^1J_{C2'H2''}$	129.931	2.694	0.094	132.719	2.127	0.172	132.230
6	$^1J_{C2'H2'}$	127.123	1.262	0.147	128.532	1.703	0.155	128.982
7	$^1J_{C3'C4'}$	31.813	1.724	0.085	33.622	0.528	0.265	32.606
8	$^1J_{C3'H3'}$	142.163	1.720	0.218	144.100	2.133	0.428	144.724
9	$^1J_{C4'C5'}$	41.282	−1.038	−0.124	40.120	0.011	−0.581	40.711
10	$^1J_{C4'H4'}$	135.707	−0.602	0.217	135.322	1.474	−0.182	137.000
11	$^1J_{C5'H5'}$	134.794	5.671	0.484	140.949	2.924	1.390	139.109
12	$^1J_{C5'H5''}$	130.096	3.906	0.607	134.609	2.486	0.847	133.429
13	$^1J_{C8N9}$	6.370	−0.115	−0.225	6.029	−0.242	−0.333	5.795
14	$^1J_{C5N9}$	10.610	−0.221	−0.178	10.211	−0.219	−0.286	10.105
15	$^1J_{C8N7}$	−0.890	−0.486	−0.272	−1.648	−0.399	−0.458	−1.747
16	$^1J_{C8H8}$	200.018	2.714	1.670	204.402	2.673	2.964	205.654
17	$^1J_{C5N7}$	−3.195	−0.397	−0.356	−3.947	−0.344	−0.631	−4.170
18	$^1J_{C4C5}$	72.371	−0.134	−0.090	72.147	−0.734	−0.161	71.477
19	$^1J_{C5H5}$	179.193	2.884	1.082	183.159	2.371	1.982	183.545
20	$^1J_{C4H4}$	178.125	1.923	1.261	181.309	1.526	2.198	181.849
21	$^2J_{C1'C3'}$	1.246	0.030	−0.009	1.267	−0.074	−0.023	1.148
22	$^2J_{C1'H2''}$	1.939	−0.295	0.000	1.644	−0.282	0.004	1.661
23	$^2J_{C1'H2'}$	−6.095	−0.365	0.033	−6.427	−0.371	0.015	−6.450
24	$^2J_{C1'C4'}$	1.995	−0.029	−0.074	1.892	−0.018	−0.059	1.918
25	$^2J_{C1'C8}$	1.586	−0.032	−0.053	1.501	−0.043	−0.123	1.420
26	$^2J_{C1'C4}$	4.302	0.069	−0.094	4.278	0.072	−0.045	4.329
27	$^2J_{C2'H1'}$	−0.133	−0.119	−0.027	−0.280	−0.196	0.056	−0.274
28	$^2J_{C2'C4'}$	0.210	0.037	0.030	0.277	−0.019	0.000	0.190
29	$^2J_{C2'N9}$	0.373	−0.052	0.009	0.330	−0.023	−0.010	0.340
30	$^2J_{C2'H3'}$	−0.434	0.182	0.022	−0.230	−0.181	0.082	−0.533
31	$^2J_{H2'H2''}$	−12.941	−0.447	−0.040	−13.428	−0.538	0.033	−13.446
32	$^2J_{C3'H2''}$	−4.811	−0.212	−0.024	−5.047	−0.301	0.019	−5.094
33	$^2J_{C3'H2'}$	−0.581	−0.649	0.029	−1.200	−0.366	0.002	−0.944
34	$^2J_{C3'H(O3')}$	−2.382	−1.665	−0.022	−4.068	−0.516	−0.227	−3.124
35	$^2J_{C3'C5'}$	0.816	0.087	0.037	0.940	−0.020	0.047	0.843
36	$^2J_{C3'H4'}$	−4.443	−0.265	−0.017	−4.725	−0.302	0.007	−4.739
37	$^2J_{C4'H3'}$	5.947	−0.525	−0.005	5.417	−0.208	−0.126	5.613
38	$^2J_{C4'H5'}$	−5.350	0.054	0.015	−5.281	−0.310	0.140	−5.521
39	$^2J_{C4'H5''}$	3.179	0.254	0.085	3.519	−0.166	0.109	3.123
40	$^2J_{C5'H(O5')}$	−2.472	−4.448	−0.081	−7.001	−0.861	−1.114	−4.447
41	$^2J_{H5'H5''}$	−9.481	−1.279	0.052	−10.707	−0.450	−0.280	−10.210
42	$^2J_{N9H8}$	5.337	0.178	0.100	5.616	0.083	0.168	5.589
43	$^2J_{N9H4}$	3.058	0.011	0.105	3.175	0.005	0.193	3.256
44	$^2J_{N9N7}$	−1.001	0.002	0.006	−0.994	0.006	0.016	−0.979
45	$^2J_{N9C5}$	4.626	−0.059	−0.013	4.554	−0.067	−0.020	4.538
46	$^2J_{C5C8}$	−3.413	−0.448	−0.113	−3.974	−0.423	−0.173	−4.008
47	$^2J_{C4C8}$	11.748	0.274	0.025	12.047	0.128	0.021	11.897
48	$^2J_{N7H8}$	8.584	0.352	0.072	9.009	0.186	0.141	8.911
49	$^2J_{N7H5}$	7.321	0.361	0.067	7.748	0.171	0.144	7.635
50	$^2J_{N7C4}$	−1.545	−0.104	−0.007	−1.656	−0.085	−0.010	−1.640
51	$^2J_{C5H4}$	9.088	−0.174	0.025	8.939	−0.151	0.009	8.947
52	$^2J_{C4H5}$	16.862	0.320	−0.050	17.132	0.027	−0.096	16.793
53	$^3J_{C1'H3'}$	6.643	0.512	−0.044	7.110	0.276	−0.016	6.903
54	$^3J_{C1'C5'}$	0.127	0.023	−0.015	0.135	−0.003	0.028	0.152
55	$^3J_{C1'H4'}$	3.494	0.041	0.121	3.656	0.091	−0.011	3.574
56	$^3J_{C1'H8}$	0.530	0.011	−0.029	0.511	0.014	−0.039	0.505
57	$^3J_{C1'H4}$	2.011	0.080	−0.091	2.000	0.064	−0.156	1.919
58	$^3J_{C1'N7}$	−0.149	−0.005	−0.007	−0.161	0.001	−0.014	−0.163
59	$^3J_{C1'C5}$	4.273	0.060	−0.034	4.299	0.025	−0.039	4.259
60	$^3J_{C2'H(O3')}$	8.482	−0.056	0.001	8.426	0.072	−0.097	8.457

Table 4. Continued

N	bond path	$J_0^{(a)}$	$\bar{J}^{(a)}_{ZPV}$	$\bar{J}^{(a)}_{thermal}$	$\bar{J}^{(a)}$	$\bar{J}^{(a)}_{ZPV,harmonic}$	$\bar{J}^{(a)}_{thermal,harmonic}$	$\bar{J}^{(a)}_{harmonic}$
61	$^3J_{C2'J4'}$	0.999	−0.095	0.046	0.949	0.028	0.001	1.028
62	$^3J_{C2'C8}$	1.096	0.107	0.071	1.274	0.089	0.051	1.236
63	$^3J_{C2'C4}$	0.930	0.011	0.062	1.003	0.028	0.009	0.967
64	$^3J_{H1'H2''}$	5.690	0.328	0.053	6.071	0.274	−0.044	5.920
65	$^3J_{H1'H2'}$	8.356	1.097	−0.041	9.412	0.735	−0.017	9.074
66	$^3J_{C3'H1'}$	0.072	0.051	0.006	0.130	0.049	0.032	0.153
67	$^3J_{C3'H5'}$	7.010	0.367	0.015	7.392	0.290	−0.019	7.281
68	$^3J_{C3'H5''}$	0.874	0.217	0.022	1.113	0.108	0.048	1.031
69	$^3J_{C3'N9}$	0.900	0.007	−0.010	0.897	0.014	−0.005	0.908
70	$^3J_{H3'H(O3')}$	1.368	1.506	0.038	2.913	0.370	0.252	1.989
71	$^3J_{C4'H2''}$	3.766	0.057	−0.049	3.775	0.143	−0.039	3.870
72	$^3J_{C4'H2'}$	0.229	0.125	0.036	0.390	0.071	0.038	0.338
73	$^3J_{C4'H(O3')}$	0.255	0.357	−0.022	0.590	0.033	0.050	0.337
74	$^3J_{C4'H(O5')}$	7.146	−0.536	−0.186	6.424	−0.033	−0.266	6.848
75	$^3J_{C4'N9}$	0.550	0.013	−0.027	0.537	−0.003	−0.001	0.547
76	$^3J_{C5'H3'}$	2.053	0.164	0.007	2.224	0.074	0.018	2.145
77	$^3J_{H4'H5'}$	2.284	−0.125	0.017	2.176	0.037	−0.045	2.276
78	$^3J_{H4'H5''}$	1.878	−0.030	−0.021	1.827	−0.019	−0.004	1.855
79	$^3J_{H5'H(O5')}$	4.211	3.374	0.221	7.806	0.528	0.745	5.484
80	$^3J_{H5''H(O5')}$	−0.557	7.782	0.017	7.242	1.175	2.094	2.712
81	$^3J_{H2''H3'}$	0.307	0.102	0.002	0.412	0.078	0.022	0.408
82	$^3J_{H2'H3'}$	5.388	0.179	0.025	5.593	0.188	−0.051	5.525
83	$^3J_{H3'H4'}$	0.024	0.137	0.026	0.187	0.082	0.035	0.142
	$^{2h}J_{C5'H8}$	0.008	−0.012	−0.002	−0.006	−0.003	−0.004	0.001

[a] All values are in units of Hz.

Table 5. Calculated Fitting Parameters for the Chemical Shielding of Selected Atoms in IDR Displaced along the ν_{69} Vibrational Coordinate

atom	$\sigma^{(A)}(-\alpha)$	$\sigma^{(A)}(-0.5\alpha)$	$\sigma^{(A)}(+0.5\alpha)$	$\sigma^{(A)}(+\alpha)$	$\sigma_1^{(A)}$	$\sigma_2^{(A)}$
C1′	88.8392	88.8324	88.8196	88.8137	-1.28×10^{-2}	5.71×10^{-4}
C2′	137.5414	137.5044	137.4377	137.4080	-6.67×10^{-2}	4.89×10^{-3}
C3′	101.5085	101.5429	101.6175	101.6579	7.47×10^{-2}	4.00×10^{-3}
C4′	88.0081	87.8842	87.6261	87.4879	-2.60×10^{-1}	-9.46×10^{-3}
C5′	114.5899	114.0504	112.8476	112.1773	−1.21	-8.71×10^{-2}
H1′	25.7179	25.7174	25.7169	25.7171	-4.20×10^{-4}	4.86×10^{-4}
H2′	29.6025	29.6024	29.6031	29.6040	6.62×10^{-3}	2.14×10^{-3}
H2″	29.2763	29.2781	29.2846	29.2896	7.40×10^{-4}	6.57×10^{-4}
H3′	27.2229	27.2170	27.2079	27.2050	-8.98×10^{-3}	2.03×10^{-3}
H(O3′)	31.5940	31.5865	31.5717	31.5643	-1.48×10^{-2}	5.71×10^{-5}
H4′	27.9821	27.9873	27.9964	28.0002	9.06×10^{-3}	-9.43×10^{-4}
H5′	27.9060	27.8582	27.7422	27.6728	-1.16×10^{-1}	-1.43×10^{-2}
H5″	28.0140	27.9689	27.8620	27.7995	-1.07×10^{-1}	-1.16×10^{-2}
H(O5′)	35.4773	33.3906	30.0602	28.7362	−3.36	5.08×10^{-1}

purely electronic value. This trend can be rationalized by considering that a vibrating, moving atom will be less able to effectively screen an applied magnetic field than a stationary atom; hence, we expect $\bar{\sigma}^{(A)}_{ZPV} < 0$ in all cases. The ZPV effect is comparatively larger on carbon atoms than hydrogen atoms, because of the larger number of vibrational degrees of freedom available to carbon atoms than that to hydrogen atoms.

Upon inspection of the J_0 and $\bar{J}^{(a)}_{ZPV}$ data in Table 4, we see that $^1J_{CH}$ and $^1J_{CC}$ tend to increase (except for $^1J_{C4C5}$), and $^1J_{CN}$ tends to decrease, upon ZPV correction. For the two-bond coupling constants, all ^2J values tend to decrease; however, there are more exceptions. In evaluating three-bond coupling, there is no consistent upward or downward trend,

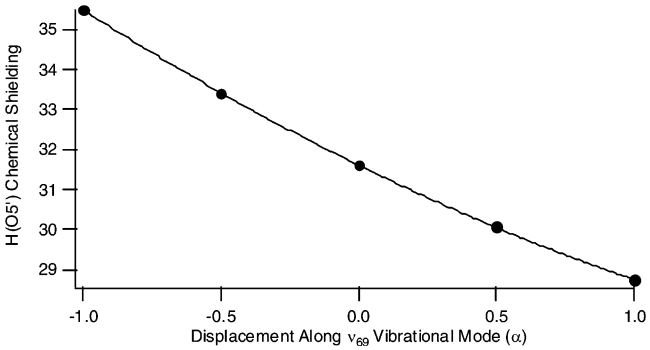

Figure 2. H(O5′) chemical shielding vs displacement along ν_{69}, in units of α. Circles: Calculated points. Line: Fit to eq 2.

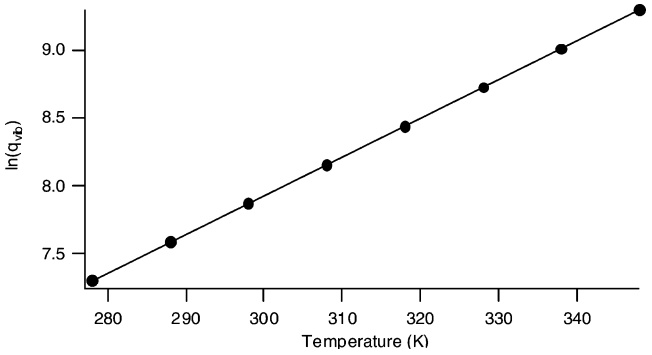

Figure 3. Dependence of the vibrational partition function on temperature for IDR in the range $T = 278-348$ K. Circles: Calculated points. Line: Fit to a straight line.

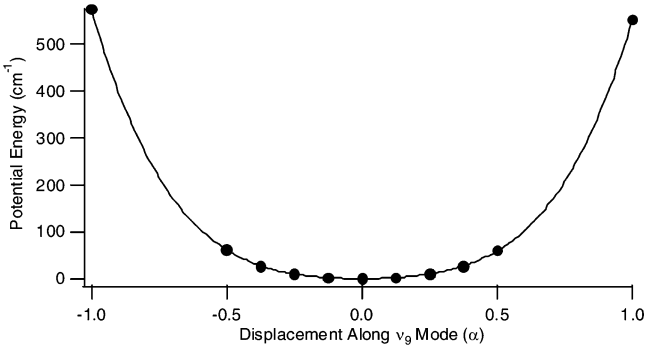

Figure 4. Potential energy curve for displacement along ν_9. Circles: Calculated points. Line: Fit to eq 1 with $\beta_9 = 134.4$ cm^{-1}, $\gamma_9 = -11.7$ cm^{-1}, and $\delta_9 = 429.1$ cm^{-1}.

one way or another. This lack of a trend may simply be due to the fact that three-bond coupling is relatively weak, and any consistent influence on ^3J values may not manifest itself in the data.

The next two columns in Tables 4 and 5 display the thermal excitation contribution and the thermal average of the chemical shielding and J coupling values, respectively. We calculate $q_{vib} = 2611$ at 298 K; the dependence of the vibrational partition function on temperature is shown in Figure 3. This large value for q_{vib} is the result of several low-lying vibrational states; as expected, states with energies below 2000 cm^{-1} overwhelmingly dominate the vibrational average. As expected, $\ln(q_{vib})$ depends linearly on the temperature in the region near room temperature; we find a slope of 0.0284 K^{-1}. When thermal averaging is included to obtain average values of σ and J, we see that, as expected, σ decreases even further; all $\bar{\sigma}^{(A)}_{thermal}$ values are negative. Again, more vibrational activity leads to less efficient screening of the magnetic field. The trend among J couplings is mixed, as before, but in general, larger vibrational effects are observed for couplings across flexible bonds (e.g., $^1J_{C8H8}$, $^2J_{C5'H(O5')}$). We also note that the calculated value of $^{2h}J_{C5'}$H8 is 0.008 Hz, decreasing to -0.006 Hz upon ZPV and thermal excitation correction, which we consider to be, for all intents and purposes, negligible.

Also presented in Tables 4 and 5 are the same thermally averaged chemical shielding/J coupling data for IDR, assuming each vibration is purely harmonic. These data are presented to illustrate the effect of the application of first-order perturbation theory to the vibrational wave functions. For the chemical shielding, we see that the effect is to increase the magnitude of $\bar{\sigma}^{(A)}_{ZPV}$ but to decrease the magnitude of $\bar{\sigma}^{(A)}_{thermal}$. This is due to the fact that the perturbed energy levels are increased compared to their harmonic values. As a result, because the vibrational ground states increase in energy, the ZPV correction becomes larger in magnitude, but because the vibrational excited states also increase in energy, fewer excited states are thermally accessible, and the thermal excitation correction becomes smaller in magnitude. Overall, the net effect is to reduce $\bar{\sigma}^{(A)}$ compared to its harmonic value (with only one exception, N9). It is also notable that the range of vibrational corrections is very wide. The correction to the carbon shielding is as small as 2.2 ppm for C1′ and as large as 8.8 ppm for C5′. The biggest single contributor to the chemical shielding vibrational correction for C1′ is the ZPV contribution from ν_{62}, corresponding to the C1′−H1 stretch mode, a comparatively high-energy vibrational mode. Conversely, the biggest contributors to the chemical shielding vibrational correction for C5′ are low-energy vibrational modes, particularly ν_6, which is a C5′−O5′−H(O5′) bending mode. Corrections to the proton shielding are smaller and more uniform, except for the OH protons. The effect of first-order perturbation theory on the chemical shielding is particularly significant for H(O3′) and H(O5′) because of two particular modes, ν_6 and ν_9. These two modes represent the C−O−H bending modes for H(O5′) and H(O3′), respectively. Shown in Figure 4 is the potential energy for displacement along the ν_9 mode. Clearly, the data indicate that this mode is highly anharmonic; a fit to a quadratic function is very poor.

In comparing the calculated thermally averaged J coupling data with the experiment, it is most fruitful to compare the $^3J_{HH}$ data, because these couplings have been the most thoroughly studied in connection with the furanose ring conformation. It would be impossible in this limited space to compare the present results with the wealth of experimental data that exist for J couplings of DNA fragments. Hence, we limit our comparisons only to free 2′-deoxyadenosine (dA) and 2′-deoxyguanosine (dG) in solution[49] and to a typical set of experimental data obtained from purine nucleosides in a self-complementary double-stranded DNA decamer, d(CCGAATCGG)$_2$.[50] This DNA fragment has a B-DNA conformation in solution and is not known to form exotic structures such as hairpin loops. The terminal G residue was omitted from the comparison owing to the conformational flexibility available for terminal groups. Shown in Table 6 is a comparison of the relevant $^3J_{HH}$ values. For the H1′−H2′ and H1′−H2″ coupling, we see that there is reasonable agreement with the experiment, both with free dA and dG and with the DNA decamer. However, for the H2′−H3′ and H2″−H3 couplings, agreement with the free dA and dG data is poor. The same poor agreement is seen with the H4′−H5′ and H4′−H5″ three-bond couplings. We believe that these discrepancies arise mainly from the neglect of contributions from other pseudorotational conformers. In solution, free nucleosides are able to adopt many conformations, including C3′-endo and -syn; the measured J couplings are therefore statistical averages over all of the conformations

Table 6. Comparison of Calculated $\bar{J}$ with Experiment at $T = 298$ K

bond path	calculated $\bar{J}$ (Hz)	dA[a] (Hz)	dG[a] (Hz)	dA[b] (Hz)	dA[c] (Hz)	dG[d] (Hz)	dG[e] (Hz)
$^3J_{H1'H2''}$	6.071	7.7	7.3	5.4	6.2	5.0	5.3
$^3J_{H1'H2'}$	9.412	6.2	6.5	9.5	8.5	10.4	9.6
$^3J_{H2''H3'}$	0.412	6.1	6.3	2.7	2.4	1.5	2.0
$^3J_{H2'H3'}$	5.593	3.3	3.6	n/a	5.3	5.6	6.2
$^3J_{H1'H2'} + {}^3J_{H1'H2''}$	15.483	13.9	13.8	14.9	14.7	15.4	14.9
$^3J_{H2'H3'} + {}^3J_{H2''H3'}$	6.005	9.4	9.9	n/a	7.7	7.1	8.2
$^3J_{H3'H4'}$	0.187	3.0	3.2				
$^3J_{H4'H5'}$	2.176	3.3	3.6				
$^3J_{H4'H5''}$	1.827	4.3	4.7				

[a] Free dA/dG in solution, from ref 49. [b] dA(4) in a d(CCGAATTCGG)$_2$ duplex decamer, from ref 50. [c] dA(5) in a d(CCGAATTCGG)$_2$ duplex decamer, from ref 50. [d] dG(3) in a d(CCGAATTCGG)$_2$ duplex decamer, from ref 50. [e] dG(9) in a d(CCGAATTCGG)$_2$ duplex decamer, from ref 50.

Table 7. Comparison of Calculated Vicinal $^3J_{HH}$ Coupling Constants with the Haasnoot Equation

bond path	HCCH dihedral angle (deg)	calculated $\bar{J}$ (Hz)	J[a] (Hz)
$^3J_{H1'H2''}$	32.16	6.071	6.25
$^3J_{H1'H2'}$	154.27	9.412	9.47
$^3J_{H2''H3'}$	86.95	0.412	0.53
$^3J_{H2'H3'}$	−34.53	5.593	6.10
$^3J_{H3'H4'}$	−99.13	0.187	1.20
$^3J_{H4'H5'}$	−64.87	2.176	3.57
$^3J_{H4'H5''}$	52.68	1.827	1.38

[a] From eq 16.

present. In the present study, on the other hand, we have considered only the C2′-endo (south) conformation of the furanose ring. These J couplings are obviously strongly dependent on the conformation of the ring; indeed, it is somewhat surprising that the H1′−H2′ and H1′−H2″ J coupling agreement is so good. When the calculated data are compared to the experimental DNA J coupling data, agreement is much better, although quantitative agreement for $^3J_{H2''H3'}$ is still lacking.

It is also instructive to compare the calculated values with those obtained from empirical, Karplus-like equations in common use. The most relevant of these is the Haasnoot equation for $^3J_{HH}$ between two sp^3 carbon centers,[51] given by eq 11.

$$^3J_{HH} = 13.70\cos^2\phi - 0.73\cos\phi + \sum_i \Delta\chi_i[0.56 - 2.47\cos^2(s_i\phi + 16.9|\Delta\chi_i|)] \quad (16)$$

In this equation, ϕ is the H−C−C−H dihedral angle and $\Delta\chi_i = \Delta\chi_i^{\alpha} - 0.14\sum \Delta\chi_i^{\beta}$ is the difference in group electronegativity between the ith substituent and hydrogen (1.3 for O, 0.4 for C, and 0.85 for N), corrected for α and β substituents; the sum over i runs over all carbon group substituents, and s_i is the "substituent orientation factor" (cf. Figure 2 of ref 51), either +1 or −1. Shown in Table 7 is a comparison of the relevant $^3J_{HH}$ values. We see that, for these $^3J_{HH}$ values, the Haasnoot equation tends to overestimate the J coupling compared to the quantum chemical results. This discrepancy between the calculated DFT values and those predicted by eq 16 may be attributable to several factors: (1) the lack of inclusion of solvent effects in the DFT calculations, (2) the incomplete inclusion of electron correlation, and (3) the inability of the current parametrization of the Haasnoot equation to correctly model the unique torsional behavior in nucleosides.

Conclusion

We have developed a method, based on ab initio calculations and first-order perturbation theory, to include thermal averaging in calculated magnetic properties, such as chemical shielding and J couplings. We have computed chemical shielding values and many J couplings for 1′-imidazolyl-2′-deoxy-β-ribofuranose, a model compound for purine nucleosides in DNA. For IDR, as a part of our analysis, we have performed a detailed vibrational analysis at the density functional level of theory with a large basis set, an analysis which was lacking previously. We find reasonable agreement between the calculated harmonic vibrational frequencies and measured solution values in DNA. We have shown that the inclusion of thermal averaging can drastically affect the calculated values of the magnetic properties, as compared to the purely electronic values. A comparison of the J coupling data to typical results from DNA fragments shows good agreement; a comparison to isolated dA/dG molecules in solution, however, is poor. We believe this poor agreement is due to a lack of consideration of more low-energy conformers (e.g., C3′-endo and -syn) in our model system. A comparison of our results with empirical Karplus-like relationships, such as the Haasnoot equation, illustrates a systematic underestimation of present results with the empirically derived ones. It is not clear whether this trend is due to a failure of the DFT calculations or a failure of the empirical relationship to correctly predict the J coupling properties of sugar protons in nucleosides.

As a side benefit of our work, in IDR, we have also analyzed the reported "hydrogen bond" that exists between H8 of the imidazole ring and O5′ on the sugar moiety. We find that the structural and magnetic data lending support to the notion of a hydrogen bond are weak; we believe that this interaction should more properly be characterized as a dipole−dipole interaction.

To improve upon our results, we believe more structural features should be added to the model compound, such as phosphate groups, to more closely model actual B-DNA strands. Also, even though a particular DNA strand may consist predominantly of B-DNA conformers, there may be a small population of A-DNA conformers that also contribute to the measured NMR response; an analysis of the A-DNA conformer, along with suitable statistical averaging, should also improve the agreement between theory and the experiment.

One additional problem arises because a Cartesian normal-mode analysis leads to errors in computing the effects of torsional modes. Treatment of the torsion about bonds as strictly linear Cartesian displacements normal to the bond leads to alteration in bond distances at high displacements, and corrections for such effects would require the introduc-

tion of anharmonic mode couplings, which greatly increases the computational time needed. However, in the present instance, the glycosidic and exocyclic torsions both involve heavy atom displacements, which means the vibrational amplitudes are rather small. The most serious errors, therefore, are likely to be on O−H proton chemical shifts, where the torsional modes introduce a second-order increase in the O−H bond length, which likely results in an artifactual reduction in the computed chemical shielding of the proton. However, OH proton chemical shifts are often difficult to measure, and two of the three OH protons are absent in RNA as a result of esterification. This error, therefore, is likely of limited practical impact, but we caution that any comparison of the present result with computed OH chemical shifts should bear this effect in mind.

Acknowledgment. J.N.W. would like to acknowledge the assistance of Professor Stephen Tanner, Department of Mathematics at Eastern Oregon University, and Mr. Xiongjian Wu, Department of Chemistry at University of Nebraska—Lincoln, in the computation of thermal averages. We gratefully acknowledge the financial support of the National Institutes of Health (R01 GM 065252).

Appendix

To evaluate the infinite sums in eqs 4 and 5, one must first compute the integrals $\langle\psi_m^{(0)}|\hat{y}|\psi_n^{(0)}\rangle$, $\langle\psi_m^{(0)}|\hat{y}^2|\psi_n^{(0)}\rangle$, $\langle\psi_m^{(0)}|\hat{y}^3|\psi_n^{(0)}\rangle$, and $\langle\psi_m^{(0)}|\hat{y}^4|\psi_n^{(0)}\rangle$ that appear repeatedly. These integrals may be solved using standard quantum-mechanical operator and integration techniques to yield the following expressions, found in common quantum-mechanical textbooks.

$$\langle\psi_m^{(0)}|\hat{y}|\psi_n^{(0)}\rangle = \sqrt{\frac{n}{2}}\delta_{m,n-1} + \sqrt{\frac{n+1}{2}}\delta_{m,n+1} \quad (17)$$

Then, one substitutes these integrals into the expressions for

$$\langle\psi_m^{(0)}|\hat{y}^2|\psi_n^{(0)}\rangle = \frac{1}{2}\sqrt{n(n-1)}\delta_{m,n-2} + \left(n+\frac{1}{2}\right)\delta_{m,n} + \frac{1}{2}\sqrt{(n+1)(n+2)}\delta_{m,n+2} \quad (18)$$

$$\langle\psi_m^{(0)}|\hat{y}^3|\psi_n^{(0)}\rangle = \sqrt{\frac{n(n-1)(n-2)}{8}}\delta_{m,n-3} + \frac{3n}{2}\sqrt{\frac{n}{2}}\delta_{m,n-1} + \frac{3(n+1)}{2}\sqrt{\frac{n+1}{2}}\delta_{m,n+1} + \sqrt{\frac{(n+1)(n+2)(n+3)}{8}}\delta_{m,n+3} \quad (19)$$

$$\langle\psi_m^{(0)}|\hat{y}^4|\psi_n^{(0)}\rangle = \frac{1}{4}\sqrt{n(n-1)(n-2)(n-3)}\delta_{m,n-4} + \sqrt{n(n-1)}\left(n-\frac{1}{2}\right)\delta_{m,n-2} + \frac{3}{2}\left(n^2+n+\frac{1}{2}\right)\delta_{m,n} + \sqrt{(n+1)(n+2)}\left(n+\frac{3}{2}\right)\delta_{m,n+2} + \frac{1}{4}\sqrt{(n+1)(n+2)(n+3)(n+4)}\delta_{m,n+4} \quad (20)$$

$c_{j,nm}^{(1)}$, $\langle\sigma_{1j}^{(A)}\rangle_n$, and $\langle\sigma_{2j}^{(A)}\rangle_n$ and evaluates the sums directly. Because of the Kronecker δ's, only a limited number of terms remain in each sum. The result for each sum is a complex polynomial in n. Define $\gamma_{r,j} = \gamma_j/\hbar\omega_{0j}$ and $\delta_{r,j} = \delta_j/\hbar\omega_{0j}$ as the reduced cubic and quartic potential energy fitting coefficients for the jth mode, respectively. The sums become:

$$\sum_{m\neq n}|c_{j,nm}^{(1)}|^2 = \frac{{\gamma_{r,j}}^2}{36}\left(n+\frac{1}{2}\right)(82n^2+82n+87) + \frac{{\delta_{r,j}}^2}{128}(65n^4+130n^3+487n^2+422n+156) \quad (21)$$

$$\langle\sigma_{1j}^{(A)}\rangle_n = \frac{\sigma_1^{(A)}\gamma_{r,j}}{1+\sum_{m\neq n}(c_{j,nm}^{(1)})^2}\left[\frac{\delta_{r,j}}{16}(27n^4+54n^3+177n^2+150n+52) - 3\left(n+\frac{1}{2}\right)\right] \quad (22)$$

$$\langle\sigma_{2j}^{(A)}\rangle_n = \frac{\sigma_2^{(A)}}{1+\sum_{m\neq n}(c_{j,nm}^{(1)})^2} \times \left[\left(n+\frac{1}{2}\right) - 3\delta_{r,j}\left(n^2+n+\frac{1}{2}\right) + \frac{{\gamma_{r,j}}^2}{144}(202n^4+404n^3+1478n^2+1276n+393) + \frac{{\delta_{r,j}}^2}{256}(146n^5+365n^4+2704n^3+3691n^2+3438n+1116)\right] \quad (23)$$

Supporting Information Available: Equilibrium coordinates for IDR; isotropic chemical shifts as a function of displacement along each mode; isotropic J couplings as a function of displacement along each mode; equilibrium structure shielding and the zero-point and thermal corrections to the shielding, for each atom; equilibrium structure J couplings and the zero-point and thermal corrections to the couplings, for each atom; equilibrium values of the chemical shift and J coupling for each atom or pair of atoms; and the C program used to calculate the perturbation corrections to the shielding and J couplings. This information is available free of charge via the Internet at http://pubs.acs.org.

References

(1) (a) Cavanaugh, J. *Protein NMR Spectroscopy: Principles and Practice*; Academic Press: San Diego, CA, 1996. (b) Clore, G. M.; Gronenbom, A. M. *NMR of Proteins*; CRC Press: Boca Raton, FL, 1993. (c) Wüthrich, K. *NMR of Proteins and Nucleic Acids*; Wiley: New York, 1986. (d) Evans, J. N. S. *Biomolecular NMR Spectroscopy*; Oxford University Press: New York, 1995.

(2) Karplus, M. J. *J. Chem. Phys.* **1959**, *30*, 11−15.

(3) Karplus, M. J. *J. Am. Chem. Soc.* **1963**, *85*, 2870−2871.

(4) Džakula, Ž.; Westler, W. M.; Edison, A. S.; Markley, J. L. *J. Am. Chem. Soc.* **1992**, *114*, 6195−6199.

(5) Džakula, Ž.; DeRider, M. L.; Markley, J. L. *J. Am. Chem. Soc.* **1996**, *118*, 12796−12803.

(6) Wu, A.; Cremer, D. *J. Phys. Chem. A* **2003**, *107*, 1797−1810.

(7) Dziembowska, T.; Hansen, P. E.; Rozwadowski, Z. *Prog. Nucl. Magn. Reson. Spectrosc.* **2004**, *45*, 1−29.

(8) Vidossich, P.; Piana, S.; Miani, A.; Carloni, P. *J. Am. Chem. Soc.* **2006**, *128*, 7215−7221.

(9) Limbach, H.-H.; Denisov, G. S.; Golubev, N. S. In *Isotope Effects in Chemistry and Biology*; Kohn, A., Ed.; CRC Press: Boca Raton, FL, 2006; pp 193−230.

(10) Servis, K. L.; Domenick, R. L. *J. Am. Chem. Soc.* **1986**, *108*, 2211−2214.

(11) Freedberg, D. I.; Kopelevich, M.; Anet, F. A. L. *J. Phys. Org. Chem.* **2001**, *14*, 625−635.

(12) Burgi, R.; Pitera, J.; van Gunsteren, W. F. *J. Biomol. NMR* **2001**, *19*, 305−320 and references therein.

(13) Case, D. A.; Scheurer, C.; Brüschweiler, R. A. *J. Am. Chem. Soc.* **2000**, *122*, 10390−10397.

(14) Markwick, P. R. L.; Sprangers, R.; Sattler, M. *J. Am. Chem. Soc.* **2003**, *125*, 644−645.

(15) Foloppe, N.; MacKerell, A. D., Jr. *J. Phys. Chem. B* **1998**, *102*, 6669−6678.

(16) Leulliot, N.; Ghomi, M.; Scalmani, G.; Berthier, G. *J. Phys. Chem. A* **1999**, *103*, 8716−8724.

(17) Moreno, M.; Douhal, A.; Lluch, J. M.; Castano, O.; Frutos, L. M. *J. Phys. Chem. A* **2001**, *105*, 3887−3893.

(18) Casadesus, R.; Moreno, M.; Lluch, J. M. *Chem. Phys.* **2003**, *290*, 319−336.

(19) Gelabert, R.; Moreno, M.; Lluch, J. M. *J. Phys. Chem. A* **2006**, *110*, 1145−1151.

(20) Bertran, J.; Oliva, A.; Rodriguez-Santiago, L.; Sodupe, M. *J. Am. Chem. Soc.* **1998**, *120*, 8159−8167.

(21) Kuo, I. F.; Tobias, D. J. *J. Phys. Chem. B* **2001**, *105*, 5827−5832.

(22) Schwegler, E.; Galli, G.; Gygi, F. *Chem. Phys. Lett.* **2001**, *342*, 434−440.

(23) Chen, X. H.; Zhang, J. Z. H. *J. Chem. Phys.* **2004**, *120*, 11386−11391.

(24) Barone, G.; Saturnino, C.; DeMartino, G.; Duca, D.; La-Manna, G. *THEOCHEM* **2001**, *572*, 113−119.

(25) Del Bene, J. E.; Jordan, M. J. T.; Perera, A.; Bartlett, R. J. *J. Phys. Chem. A* **2001**, *105*, 8399−8402.

(26) Del Bene, J. E.; Jordan, M. J. T. *J. Phys. Chem. A* **2002**, *106*, 5385−5392.

(27) Grigoleit, S.; Bühl, M. *Chem.—Eur. J.* **2004**, *10*, 5541−5552.

(28) Nielsen, P. A.; Norrby, P.; Liljefors, T.; Rega, N.; Barone, V. *J. Am. Chem. Soc.* **2000**, *122*, 3151−3155.

(29) Case, D. A. *J. Biomol. NMR* **1999**, *15*, 95−102.

(30) Schmidt, M. W.; Baldridge, K. K.; Boatz, J. A.; Elbert, S. T.; Gordon, M. S.; Jensen, J. H.; Koseki, S.; Matsunaga, N.; Nguyen, K. A.; Su, S. J.; Windus, T. L.; Dupuis, M.; Montgomery, J. A. *J. Comput. Chem.* **1993**, *14*, 1347−1363; version 20 JUN 2002 (R2).

(31) Baker, J.; Kessi, A.; Delley, B. *J. Chem. Phys.* **1996**, *105*, 192−212.

(32) (a) Becke, A. D. *J. Chem. Phys.* **1993**, *98*, 5648−5652. (b) Lee, C.; Yang, W.; Parr, R. G. *Phys. Rev. B: Condens. Matter Mater. Phys.* **1988**, *37*, 785−789.

(33) Frisch, M. J.; Trucks, G. W.; Schlegel, H. B.; Scuseria, G. E.; Robb, M. A.; Cheeseman, J. R.; Montgomery, J. A., Jr.; Vreven, T.; Kudin, K. N.; Burant, J. C.; Millam, J. M.; Iyengar, S. S.; Tomasi, J.; Barone, V.; Mennucci, B.; Cossi, M.; Scalmani, G.; Rega, N.; Petersson, G. A.; Nakatsuji, H.; Hada, M.; Ehara, M.; Toyota, K.; Fukuda, R.; Hasegawa, J.; Ishida, M.; Nakajima, T.; Honda, Y.; Kitao, O.; Nakai, H.; Klene, M.; Li, X.; Knox, J. E.; Hratchian, H. P.; Cross, J. B.; Adamo, C.; Jaramillo, J.; Gomperts, R.; Stratmann, R. E.; Yazyev, O.; Austin, A. J.; Cammi, R.; Pomelli, C.; Ochterski, J. W.; Ayala, P. Y.; Morokuma, K.; Voth, G. A.; Salvador, P.; Dannenberg, J. J.; Zakrzewski, V. G.; Dapprich, S.; Daniels, A. D.; Strain, M. C.; Farkas, O.; Malick, D. K.; Rabuck, A. D.; Raghavachari, K.; Foresman, J. B.; Ortiz, J. V.; Cui, Q.; Baboul, A. G.; Clifford, S.; Cioslowski, J.; Stefanov, B. B.; Liu, G.; Liashenko, A.; Piskorz, P.; Komaromi, I.; Martin, R. L.; Fox, D. J.; Keith, T.; Al-Laham, M. A.; Peng, C. Y.; Nanayakkara, A.; Challacombe, M.; Gill, P. M. W.; Johnson, B.; Chen, W.; Wong, M. W.; Gonzalez, C.; Pople, J. A. *Gaussian 03*, revision B.04; Gaussian, Inc.: Pittsburgh, PA, 2003.

(34) Foloppe, N.; Nilsson, L.; MacKerell, A. D., Jr. *Biopolymers* **2002**, *61*, 61−76.

(35) Altona, C.; Sundaralingam, M. *J. Am. Chem. Soc.* **1972**, *94*, 8205−8212.

(36) Rubin, J.; Brennan, T.; Sundaralingam, M. *Biochemistry* **1972**, *11* (1), 3112−3128.

(37) Wahyl, M. C.; Sundaralingam, M. *Trends Biochem. Sci.* **1997**, *22*, 97−102.

(38) Hocquet, A.; Ghomi, M. *Phys. Chem. Chem. Phys.* **2000**, *2*, 5351−5353.

(39) Hobza, P.; Havlas, Z. *Chem. Rev.* **2000**, *100*, 4253−4264.

(40) Hocquet, A. *Phys. Chem. Chem. Phys.* **2001**, *3*, 3192−3199.

(41) Nir, E.; Hünig, I.; Kleinermanns, K.; de Vries, M. *ChemPhysChem* **2004**, *5*, 131−137.

(42) Boatz, J. A.; Gordon, M. S. *J. Phys. Chem.* **1989**, *93*, 1819−1826.

(43) Pelmenschikov, A.; Hovorun, D. M.; Shishkin, O. V.; Leszczynski, J. *J. Chem. Phys.* **2000**, *113*, 5986−5990.

(44) Leulliot, N.; Ghomi, M.; Jobic, H.; Bouloussa, O.; Baumruk, V.; Coulombeau, C. *J. Phys. Chem. B* **1999**, *103*, 10934−10944.

(45) Nir, E.; Imhof, P.; Kleinermanns, K.; de Vries, M. S. *J. Am. Chem. Soc.* **2000**, *122*, 8091−8092.

(46) Nir, E.; Plutzer, C.; Kleinermanns, K.; de Vries, M. *Eur. Phys. J. D* **2002**, *20*, 317−329.

(47) Nir, E.; Hunig, I.; Kleinermanns, K.; de Vries, M. S. *ChemPhysChem* **2004**, *5*, 131−137.

(48) Banyay, M.; Sarkar, M.; Gräslund, A. *Biophys. Chem.* **2003**, *104*, 477−488.

(49) Plavec, J.; Tong, W.; Chattopadhyaya, J. *J. Am. Chem. Soc.* **1993**, *115* (5), 9734−9746.

(50) Rinkel, L. J.; van der Marel, G. A.; van Boom, J. H.; Altona, C. *Eur. J. Biochem.* **1987**, *163*, 175−286.

(51) Haasnoot, C. A. G.; de Leeuw, F. A. A. M.; Altona, C. *Tetrahedron* **1980**, *36*, 2783−2792.

CT6000736